This is a repository copy of *Reactive inkjet printing of functional silk stirrers for enhanced mixing and sensing*.

White Rose Research Online URL for this paper:
http://eprints.whiterose.ac.uk/139856/

Version: Accepted Version

Article:
Zhang, Y. orcid.org/0000-0002-8925-2284, Gregory, D.A. orcid.org/0000-0003-2489-5462, Zhang, Y. orcid.org/0000-0002-5861-2427 et al. (3 more authors) (2018) Reactive inkjet printing of functional silk stirrers for enhanced mixing and sensing. Small. e1804213. ISSN 1613-6810

https://doi.org/10.1002/smll.201804213

This is the peer reviewed version of the following article: Y. Zhang, D. A. Gregory, Y. Zhang, P. J. Smith, S. J. Ebbens, X. Zhao, Small 2018, 1804213, which has been published in final form at https://doi.org/10.1002/smll.201804213. This article may be used for non-commercial purposes in accordance with Wiley Terms and Conditions for Self-Archiving.

Reuse
Items deposited in White Rose Research Online are protected by copyright, with all rights reserved unless indicated otherwise. They may be downloaded and/or printed for private study, or other acts as permitted by national copyright laws. The publisher or other rights holders may allow further reproduction and re-use of the full text version. This is indicated by the licence information on the White Rose Research Online record for the item.

Takedown
If you consider content in White Rose Research Online to be in breach of UK law, please notify us by emailing eprints@whiterose.ac.uk including the URL of the record and the reason for the withdrawal request.

eprints@whiterose.ac.uk
https://eprints.whiterose.ac.uk/

DOI: 10.1002/((please add manuscript number))
Article type: Communication

Reactive Inkjet Printing of Functional Silk Stirrers for Enhanced Mixing and Sensing

*Yu Zhang, David A. Gregory, Yi Zhang, Patrick J. Smith, Stephen J. Ebbens, and Xiubo Zhao**

Dr. Y. Zhang, Dr. D. A. Gregory, Dr. Y. Zhang, Dr. S. J. Ebbens, Dr. X. Zhao

Department of Chemical and Biological Engineering, University of Sheffield, Mappin Street, Sheffield, Mappin Street, S1 3JD, UK

E-mail: xiubo.zhao@sheffield.ac.uk

Dr. P. J. Smith

Department of Mechanical Engineering, University of Sheffield, 64 Garden Street, Sheffield, 64 Garden Street, S1 4BJ, UK

Dr. X. Zhao

School of Pharmaceutical Engineering and Life Science, Changzhou University, Gehu Road, Changzhou 213164, China

Keywords: Reactive inkjet printing, silk, enzyme, stirrer, Marangoni effect

Abstract:

Stirring small volumes of solution can reduce immunoassay readout time, homogenize cell cultures and increase enzyme reactivity in bioreactors. However, at present many small scale stirring methods require external actuation, which can be cumbersome. To address this, here, reactive inkjet printing is shown to be able to produce autonomously rotating biocompatible silk-based micro-stirrers that can enhance fluid mixing. Rotary motion is generated either by release of a surface active agent (small molecular PEG) resulting in Marangoni effect, or by catalytically powered bubble propulsion. The Marangoni driven devices do not require any chemicals to be added to the fluid as the 'fuel', while the catalytically powered devices are powered by decomposing substrate molecules in solution. A comparison of Marangoni effect and enzyme powered stirrers is made. Marangoni effect driven stirrers rotate up to 600 rpm, 75-100 fold faster than enzyme driven micro-stirrers, however enzyme powered stirrers show increased longevity. Further to stirring applications, the sensitivity of the motion generation mechanisms to fluid properties allows the rotating devices to also be exploited for sensing applications, for example, acting as motion sensors for water pollution.

Introduction

The ability to produce small scale devices that can stir, and encourage mixing in small volumes of solutions has a number of potential applications. In particular, the performance of many immunoassays is currently limited by the rate at which analytes reach the molecular binding sites of the surfaces or colloids [1]. To overcome this, a method is required to impart energy to the solution to produce advection and increase transport rates

beyond the diffusion limit [2]. A further advantage of solution agitation during immunoassays is the generation of stringency forces that can increase binding selectivity [3]. Unfortunately, methods to agitate small volumes of solution currently require external power, which increases the assays complexity, and is not compatible with point of care testing, particularly in challenging environments [4-9], such as immunoassay based analytics that are currently invaluable for medical applications [10], environmental monitoring [11-13], food safety [14, 15] and chemical threat detection [16]. Additionally, stirring small volumes of fluid has been shown to increase enzyme reactivity and proliferation in micro-bioreactors, and homogenize stem cell cultures [17, 18]. In this context, here we developed miniaturised stirrer devices based on two different mechanisms (enzymatic reactions, and the Marangoni effect) that are capable of producing autonomous motion at small scales.

The potential to produce motion in fluids by chemical reactions is well established: many small-scale devices that move rapidly through fluids by decomposing dissolved chemical "fuel" molecules at their surfaces have been documented [11, 19-22]. The primary envisaged purpose for these "swimming" devices is to enable static-microfluidic tasks, such as cargo transport [23, 24]. However, the devices' motion disturbs the surrounding fluid, also providing a route to agitate small volumes. For example, Orozco et al. [25] reported that self-propelled nano-rods increased the motion of surrounding tracer particles. In this case the additional fluid motion was attributed to convection induced by the bubbles released from the nano-rods. Morales et al. [26] have also deployed bubble-propelled devices within a microwell during a protein detection assay, and claimed that the devices enhanced detection performance. However, in these studies, the motion of the "mixing" devices was chaotic and uncontrolled, and no attempt has been made to generate regular rotary motion or make devices with a size and shape that would encourage rapid fluid mixing. Although several researchers have demonstrated that the motion produced by chemically powered self-motile devices can be controlled, this has mainly targeted persistent linear motion to aid transport tasks, rather than rotation [27-29]. In examples where autonomous chemically powered rotors have been demonstrated, the devices have been only a few microns in size, and spherical, therefore, were not designed to mix the surrounding fluids [30].

In addition to catalytically driven devices, another promising motion producing method is to use a well-known physical phenomenon: the Marangoni effect. In this mechanism, motion is caused by a surface tension gradient (along a fluid-fluid interface) between two unequilibrated liquids, which causes solutes to transfer from low tension liquid to high tension liquid, hence generating a spontaneous agitation of the interface [31, 32]. By using this driving mechanism, a small solid device leaching a soluble surface-active compound will be propelled when exposed to another fluid which can dissolve the solute and generate a difference in surface tension. The driving force is caused by the surface tension gradient around the device pulling the device to the high surface tension area [33, 34]. One advantage of using this physical phenomenon to power stirrers compared to catalytic reactions is it eliminates the requirement for addition of chemical 'fuel' into the analytical fluids, therefore minimising the potential contamination or side effects introduced by the added chemical.

Here we investigate the potential to generate regular rotary motion from these phenomena, and make devices with a size and shape that will encourage rapid fluid mixing as a result of the rotatory motion. To do this we exploit further our recently demonstrated ability to use reactive inkjet printing (RIJ) to produce geometrically controllable catalytically active silk micro-devices termed bubble-propulsive silk micro-rockets [35]. Regenerated silk fibroin (RSF) micro-rockets were fabricated by inkjet printing of enzyme-blended RSF inks, which were able to decompose hydrogen peroxide (H_2O_2) to generate continuous oxygen bubbles $[2H_2O_{2(l)} \rightarrow 2H_2O_{(l)} + O_{2(g)}]$, leading to rapid motion. The attractive features of this method, in the context of fabricating stirring devices, is the ability to accurately and digitally define the overall device shape, and precisely deposit the motion producing chemical components. The former feature allows devices with shapes and sizes that are likely to mix the surrounding fluid, while the latter allows the potential to precisely control the trajectory of the device. These features are hard to achieve using other fabrication methods such as vapour deposition [36], microscale continuous optical printing [37] and solvent addition [38]. Additionally, the fabrication of functional devices (such as soft robotics) from soft materials has attracted increasing interest in the scientific and engineering communities. For example, a soft peacock spider has been fabricated using lithographic techniques.[39] RSF derived from natural worm-silk has good biocompatibility and tailorable degradability, and can support sustained enzyme activity compared with some metallic catalyst such as platinum (Pt) which can introduce biofouling [40]. Also, access to silk is easy and cheap which significantly reduces the cost of fabrication. Therefore, we extended this approach to fabricate and test devices with controlled distributions of catalytic activity that encourage rotary motion to generate a stirring effect.

In addition to the enzymatically powered bubble-propulsive micro-stirrers, we secondly fabricated catalase-free stirrers with the same geometry as the bubble-propulsive ones. In this way we report two types of small self-motile stirring devices which autonomously produce regular rotations, both fabricated using RIJ. The motion characteristics produced by each type of these stirrers and the parameters that affect the devices' motion were quantitatively investigated. For the bubble-propulsive stirrers, single-engine (asymmetrical) and dual-engine (symmetrical) devices were fabricated to investigate the effect of different locations of enzymes on the locomotion. Additionally, the effect of H_2O_2 fuel concentration on the motion of stirrers was also analysed. For Marangoni effect driven stirrers, the effect of varying surface tension of test solutions on the locomotion of stirrers was investigated. Besides, the morphology change of the surfaces of both types of stirrers before and after exposing to related solutions were also studied using scanning electron microscope (SEM). Based on these assessments, the potential applications of using these self-propulsive micro-stirring devices to encourage mixing were explored. In addition, we discuss how the sensitivity of the propulsion mechanisms on solution parameters (enzymatic substrate and surface tension) can also allow these devices to function as motion sensors, for example to provide a visual indication of water quality from small volume samples.

Results and Discussion

Enzyme powered stirrers

Figure 1(a) shows a schematic of the RIJ process for fabricating silk stirrers incorporating localised patches of catalase positioned at either one or both of two lobes that protrude at right-angles on either side (~900 µm) at the end of a catalytically inactive linear backbone (~2 mm). The height (thickness) of the stirrers was measured to be 90 µm ± 10 µm. The choice of this overall geometry and enzyme localisation was motivated by previous observations that catalase rich regions can decompose hydrogen peroxide fuel to produce bubbles of oxygen that detach and release, generating a propulsive force that produces motion away from the active regions. In the "single-engine" case the combination of device geometry and catalase position are expected to exert torque on the stirrer due to the resultant effect of the force generated at the active site and overall drag. While for the "dual-engine" case the generated forces are expected to work in opposition to drive rotations. The lobes are also hoped to encourage coupling of the rotary motion to the surrounding solution.

The layer-by-layer deposition of three different inks builds up the 3D structure of the stirrers. Each layer is deposited by sequentially printing the designed patterns of ink A, (containing RSF and polyethylene glycol (PEG_{400}) additive), ink B (containing RSF, PEG_{400} additive and catalase), and ink C (containing blue dyed methanol) (see methods in supportive information for details). As previously described in Gregory et al. [35] the methanol did not affect the enzyme activity noticeably. The PEG_{400} additive was included as it was found to play an important role in aiding bubble detachment from the device body in our previous study [35]. The distribution of catalytic activity in a given layer is therefore defined by the precise deposition of ink A and B in the defined locations, while ink C serves to transform the RSF in inks A and B from soluble random coil structure into insoluble β-sheet structure [35]. By printing with fluorescein isothiocyanate (FITC) labelled catalase, fluorescence microscopy confirmed the ability of using RIJ to deposit the FITC-labelled catalase in the desired locations, **Figure 1(b-d)**.

If these enzymatic stirrers were placed directly into aqueous solutions as printed, extremely rapid rotation of the printed devices was observed even in absence of the H_2O_2 fuel. This was resulted from the rapidly leaching out of the PEG_{400} additive contained in inks A and B, causing surface tension gradients as discussed above. This phenomenon hampered attempts to study enzymatic driven rotation, and so to assess the motion generated solely by enzymatic decomposition, the stirrers were soaked in DI water for 10 minutes, which was found to be long enough to quench the surface tension driven rotation mechanism [35]. Following this procedure, the printed structures were no longer able to generate rotation without the addition of H_2O_2. The stirrers were then placed in a series of solutions with varying concentrations of H_2O_2 to investigate their enzymatic stirring performance.

Figure 2(a) and (b) show a time-sequence of images and trajectories for single- and dual-engine stirrers in 60 mg/ml H_2O_2 solutions respectively (**Video S1** and **S2** in supporting information). Frequent bubble release occurred from the catalase containing regions, producing rotary motion, validating the selected printed

designs. For the single-engine stirrer the radius of the circling trajectory was seen to be wider than that produced by the dual-engine stirrer. Indeed, analysis of 25 trajectories for both single- and dual-engine stirrers showed that the average diameter of the trajectory circles were 2.10 ± 0.23 mm and 1.05 ± 0.15 mm respectively. This difference likely reflects that the single-engine's rotation is due to a single propulsive force vector acting against the overall drag force experienced by the stirrer, whereas the dual-engine structure frequently releases bubbles from both ends simultaneously, and generates forces that act in opposite directions, **Figure 2(c)**. The change of orientation angle (ϕ) (defined in **Figure 1(e)**) as a function of time is also compared for each structure (**Figure 2(e) and (f)**). Single-engine stirrers show a step-wise change in angle with a constant rotation direction. Very rapid evolutions of angle are followed by periods when the orientation remains constant. This observation reveals that the rotary motion is only produced when a bubble detaches from the stirrer. Such stop-start behaviour is typical for bubble release based motion. For the dual-engine stirrers, the stop times are shorter and the motion is more persistent. Here both ends generate bubbles, increasing the frequency of motion producing bubble detachment events, and so reducing the chance of periods with no motion. The dual-engine stirrer also shows a higher rotation speed (~6 rpm) than that of single-engine stirrer (~3 rpm) at the same H_2O_2 fuel concentration (60 mg/ml). This is likely due to this increased, more continuous driving force, and the tighter rotations produced by this distribution of catalyst.

Figure 2(d) shows the effect of varying the H_2O_2 concentration on some quantitative measures of rotational behaviour for the dual-engine stirrers: the end points translational velocities (Points A and B in **Figure 1(e)**) and rotational rate. A significant increase in rotation rate as a function of H_2O_2 concentration can be observed, indicating that fuel concentration can be used as a control parameter to tailor the spinning frequency. The minimum concentration of H_2O_2, which allowed the stirrers to rotate was 20 mg/ml. The propulsion force increases with the rate of the catalytic reaction due to faster bubble generation and detachment, and increasing H_2O_2 concentration led to more rapid catalase decomposition, until molecular diffusion or intrinsic catalyst reactivity limits turnover.

Catalase stirrers were also found to change morphology in the regions containing catalase, following enzymatic propulsion. Surfaces that originally appeared flat and smooth became rough and porous after 2 hours immersion in H_2O_2, **Figure 2(g-j)**. The bulges on the surface are thought to be caused during the initial formation of bubbles below the silk layers before pores opened up to allow the release of bubbles. This suggests that the motion producing enzymatic activity takes place throughout the interior of the device, rather than just at the surface, which is desirable to maximise reactivity and maintain enzyme activity. A slight shrinking of the dried stirrers was observed in the SEM images (Figure 2 g and i) after swimming, this is most likely attributed to the release of PEG from the stirrer.

Marangoni effect powered stirrers

Different to the aforementioned enzyme powered stirrers which use catalase decomposing H_2O_2 to generate bubbles and propel the stirrers, we also exploited the Marangoni effect to produce stirring. Our initial results

for enzymatic driven stirrers discussed above suggested that the PEG_{400} additive blended into the silk ink, originally intended to promote bubble release, was also able to generate a surface tension gradient in the surrounding liquid. It was found that PEG_{400} is responsible for this effect because a pure silk structure printed without this additive does not produce any rotation (**Video S3** in supporting information). This encouraged us to also print stirrers driven purely by this phenomenon, that did not contain any enzyme. **Figure 3(a)** schematically shows the printing procedures for fabrication of these Marangoni effect powered stirrers, which proceeds as described above, but without the use of the enzyme containing ink. **Figure 3(b)** shows a sequence of images for the rotation behaviour of a typical Marangoni effect powered stirrer immediately after being placed in DI water (**Video S4** in supporting information). Tracking the movement of each end of the stirrer (red and green circles) revealed a consistent rapid rotary motion which was accompanied by very little translational motion. The rotation speed generated by these stirrers is vastly faster than that observed for the enzymatic driven stirrers. The typical rotational rate for Marangoni effect powered stirrers ranges from 450 – 600 rpm, which is approximately 75 – 100 times faster than the enzymatically powered dual-engine stirrers at the fuel concentration of 60 mg/ml. One key mechanistic difference can also be observed by comparing a graph of the orientation angle against time for the surface tension driven stirrers (**Figure 4(e)** with the equivalent data for enzymatic stirrers, **Figure 2(e) and (f)**). The step wise motion discussed above for enzyme powered swimmers is now replaced by smooth, continuous rotation, which is consistent with a continuous, surface tension driven driving force rather than sporadic bubble release.

Expanding on the mechanism for this rapid rotation: as the printed silk stirrers were buoyant, they were often found at the meniscus. Consequently, when the blended PEG_{400} leaches out from the stirrers at the air-water interface, the local surface tension around the stirrers is reduced, hence, causing the Marangoni effect (see **Figure 3(b)**). The transferring of solute (PEG_{400}) from low surface tension area (surrounding stirrer) to high surface tension area (DI water) results in a surface force acting on the stirrers. As the PEG_{400} was blended in the silk ink, and the formation of insoluble silk structure (β-sheet) was uneven, we assume that the dispersion of the PEG_{400} in the final silk structure was random, therefore, the quantity of the PEG_{400} leaching out from the stirrer and the release rate is not evenly distributed along the whole stirrer. These uneven distributions cause the surface tension gradients to differ around the stirrer generating an asymmetrical force. If the unbalanced force is not at the mass centre of the stirrer, rotary motion results. Suematsu et al. [33] have also observed the similar phenomenon: they reported that using water soluble camphor can change the surface tension of solutions to generate motion, and by making devices designed to leach camphor from specific asymmetrical locations on their surface, devices translated in a well-defined direction, or exhibited circular motion. **Figure 3(c-f)** show the SEM images of the stirrers before and after exposing to DI water. No significant morphological difference was observed. This suggests that the PEG_{400} molecules diffuse through the solid structure without changing the micron scale morphology.

To confirm that the Marangoni powered stirrers produced a change of surface tension, the effect of consecutively adding 8 stirrers to initially pure DI water was monitored, **Figure 3(g)**. The surface tension

decreased consecutively with each stirrer addition, demonstrating that PEG_{400} released from each stirrer acts as a surface tension modifier. It can be noted that the decrease in surface tension was 0.7 mN/m after adding in the first stirrer, but the reduction decreased for the next 5 stirrers (0.1 – 0.2 mN/m) before a plateau surface tension value was reached and unaffected by further addition of stirrers. The reason for this is that there were no PEG_{400} molecules at the DI water surface initially, therefore, a maximum number of PEG_{400} molecules could leach out from the stirrer (due to the high concentration gradient between stirrer and DI water), and disperse onto the DI water surface before equilibrium was reached. However, additional stirrers experience a reduced driving force for diffusive release of PEG_{400} due to the increasing concentration of this molecule already in their surroundings. This is also due to the fact that relationship between surface tension reduction and the surfactant concentration is normally a logarithm effect before the critical micelle concentration (CMC) was reached, which means further reduction of surface tension will need a vast amount of PEG_{400} release which cannot be achieved by further addition of a single stirrer. This observation was also confirmed by using a Langmuir trough to monitor the change of surface pressure after adding stirrers. **Figure 3(h)** shows the change of surface pressure as a function of time. Note that a new stirrer was only added after the previous one had stopped rotating. The Marangoni stirrers gradually reduced in speed until completely stopping and simply undergoing a very slow random drift after 250 to 300 seconds. The step-wise curve clearly shows the increase in surface pressure with the addition of each stirrer. This is because the PEG_{400} molecules leached out and some of them dispersed on the DI water surface. However, this increase stopped after the sixth stirrer. Moreover, the curve also reveals that the first added stirrer had the longest rotary motion before stopping, suggesting that this stirrer could produce a surface tension gradient for the longest time before PEG_{400} release rate slowed. This agrees with the result shown in **Figure 3(g)** that the first added stirrer decreased the surface tension of DI water the most as more PEG_{400} molecules were leached out from this stirrer.

Potential applications

Having reported the phenomenological behaviour of the two variants of the silk stirring devices, we now further discuss their potential use for two different applications:

Micro-stirring

Marangoni effect powered stirrers produce rotary motion in aqueous solutions without the requirement for hydrogen peroxide fuel, and this type of stirrer also has a very high rotation speed compared to the enzyme powered stirrers, so we also investigated its potential for solution micro-stirring. **Figure 4(a)** pictorially compares the spread of blue dye, with and without the addition of a Marangoni effect stirrer. It is clear that the stirrer dramatically enhances the spread of the dye and mixes it with the surrounding solution rapidly compared to diffusion alone. **Figure 4(b)** shows the statistical comparison of the change of diameter of the dye circle as a function of time. The change of the diameter of the dye circle with added stirrer is approximately eight times bigger than that of the control after the first ten seconds, indicating the Marangoni effect powered stirrers can be potentially used as rapid stirrers that do not need any external power. In this experiment, despite the stirrer being located at the meniscus, it was clear that the entire bulk fluid was undergoing agitation, showing that Marangoni driven surface motion can also produce significant bulk fluid

movement. Because there is no need for extra chemicals to trigger the motion, this type of stirrer is promising for biomedical applications needing rapid mixing. Currently we have demonstrated mixing at rather large scales using devices that have mm dimensions, but there is great potential to print smaller devices that exploit the same mechanism to produce motion in smaller containers, such as the micro-well plates used for many assays. This could help remove diffusion limits in current immunoassays and reduce incubation times without using actuated stirring devices, thereby assisting Point of Care (POC) deployment in challenging resource or poor environments. It is worth noting that the maximum amount of PEG_{400} that can be released by a single stirrer is around 5 µg and this low level is unlikely to impede immunoassay performance.

While the enzymatic stirrers do not produce as rapid rotation rates as the Marangoni driven samples, they may also find applications for mixing and stirring. Enzymatic stirring continues for longer than the Marangoni effect and is less dependent on the surface tension of the fluid in which stirring is required. In addition, the speed of rotation, and mixing, can be controlled by varying the fuel concentration.

Micro-sensing applications

Another possible application for the type of stirring devices we report here is to use them as micron scale visual read-out devices, or sensors, for solution properties. A simple example, would be to observe the rotation rate for an enzyme powered stirrer and then infer the H_2O_2 concentration using the data shown in **Figure 2(d)**. This approach could be used to detect enzyme inhibitors that may stop rotation despite the presence of H_2O_2.

Extending this idea, here we investigate in more detail a further useful sensing function exhibited by the Marangoni effect powered stirrers. Due to the mechanism through which they produce motion, rotational rate is expected to depend on surface tension, giving the possibility to detect common surface tension modifying water pollutants such as sodium dodecyl sulphate (SDS) by easy to visualise changes in rotation rate. Indeed, **Figure 4(d)** shows the change of rotation speed as a function of time for stirrers placed in solutions with varying concentrations of SDS (from 0 – 1 mM). As the concentration of SDS increases, the initial rotation rate of stirrers decreases due to the reduced driving force (**Video S6-S10**, supporting information). Additionally, the rotation speed decreases gradually as a function of time, illustrating the surface tension gradient was dynamically reducing due to PEG_{400} leaching out from the stirrers. **Figures 4(e-h)** display corresponding orientation against time plots at selected SDS concentrations. This is a good example to prove that inkjet printed stirrers with an appropriate formulation of inks, suitable geometry etc. are promising candidates to act as visual rotation sensors for polluted water. Moreover, because no external power source is needed to trigger the motion, and the size of stirrers is tailorable, the self-propelled, portable stirrers are particularly useful for analyses need to be conducted under unfriendly conditions such as hardly accessible external power, dedicated lab equipment, limited transportation and human labour. We note that correlations between surface tension and overall water quality have been documented, and also that surface tension has been used as a criterion to confirm river water quality [41], suggesting that this approach could be of general use, and is not limited to detection of specific surface-active agents.

Conclusions

We have demonstrated the ability of using reactive inkjet printing to fabricate mm scale silk stirrers with well-defined shapes and compositions that undergo spontaneous rotation when placed in appropriate fluids. We designed and investigated two types of self-propelled stirrers:

(1) **Enzyme powered stirrers**: catalase was deposited at the predefined place(s) within a stirrer to produce bubble propelled rotation resulting from the decomposition of dissolved hydrogen peroxide in DI water. Comparison of two stirrers with different catalase distributions revealed that positioning catalase at both ends of a stirrer resulted in faster and more defined circular rotation, compared to single catalase engine stirrers. The character of the rotation produced by bubble propulsion is a start-stop motion rather than smooth, due to discrete bubble release events. The rotational rate for catalase doped stirrers can be controlled by varying H_2O_2 concentrations.

(2) **Marangoni effect powered stirrers**: surface tension gradients generated by a surface-active agent releasing from the printed stirrer also results in rotary motion. This rapid, smooth rotation at a liquid surface, also significantly enhances mixing in the bulk fluid. The mixing produced by this surface tension effect does not require the addition of chemical fuels to the solution being mixed, which are advantageous over bubble-propelled stirrers. This type of device can be potentially used as a sensor for environmental monitoring such as water quality/contamination monitoring. Trace contamination that reduces the surface tension of water will affect the devices stirring speed, where the higher the contamination levels are the slower the devices rotation is.

Overall this work provides a starting point to encourage the use of autonomous stirring functions generated by chemical decomposition and/or surface tension gradients to produce new, faster and simpler implementations of current POC analytical methods that require stirring. Further to this we illustrated the potential for these devices to act as sensors, for example to perform environmental monitoring.

Supporting Information

Supporting Information is available from the Wiley Online Library or from the author.

Acknowledgements

The authors would like to acknowledge support from the EPSRC via X. Zhao's reactive inkjet printing of silk materials awards (EP/N007174/1 and EP/N023579/1), S. J. Ebbens' Fellowship awards (EP/J002402/1 and EP/N033736/1), and P. J. Smith's reactive inkjet printing award (EP/J014850/1). X. Zhao also thanks Royal Society (RG160662) and Jiangsu specially-appointed professors program for support. The authors thank Professor Qingyou Xia from state key laboratory of silkworm genome biology, Southwest University, China for providing silk cocoons.

Received: ((will be filled in by the editorial staff))
Revised: ((will be filled in by the editorial staff))
Published online: ((will be filled in by the editorial staff))

References:

1. J. E. Butler, *Methods* **2000**, *22*, 4.
2. W. Kusnezow, Y. V. Syagailo, S. Rüffer, K. Klenin, W. Sebald, J. D. Hoheisel, C. Gauer, I. Goychuk, *Proteomics* **2006**, *6*, 794.
3. A. Van Reenen, A. M. de Jong, J. M. den Toonder, M. W. Prins, *Lab on a Chip* **2014**, *14*, 1966.

4. Y. H. Lin, Y. J. Chen, C. S. Lai, Y. T. Chen, C. L. Chen, J. S. Yu, Y. S. Chang, *Biomicrofluidics* **2013**, *7*, 024103.
5. A. Rathgeber, M. Wassermeier, A. Wixforth, *J. ASTM Int.* **2005**, *2*, 1.
6. D. De Bruyker, M. I. Recht, A. A. S. Bhagat, F. E. Torres, A. G. Bell, R. H. Bruce, *Lab on a Chip* **2011**, *11*, 3313.
7. T. Frommelt, M. Kostur, M. Wenzel-Schäfer, P. Talkner, P. Hänggi, A. Wixforth, *Phys. Rev. Lett.* **2008**, *100*, 034502.
8. K. S. Ryu, K. Shaikh, E. Goluch, Z. Fan, C. Liu, *Lab on a Chip* **2004**, *4*, 608.
9. T. Li, J. Li, H. Zhang, X. Chang, W. Song, Y. Hu, G. Shao, E. Sandraz, G. Zhang, L. Li, *Small* **2016**, *12*, 6098.
10. P. Yager, T. Edwards, E. Fu, K. Helton, K. Nelson, M. R. Tam, B. H. Weigl, *Nature* **2006**, *442*, 412.
11. L. Soler, V. Magdanz, V. M. Fomin, S. Sanchez, O. G. Schmidt, *ACS Nano* **2013**, *7*, 9611.
12. L. Soler, S. Sanchez, *Nanoscale* **2014**, *6*, 7175.
13. J. Orozco, L. A. Mercante, R. Pol, A. Merkoçi, *J. Mater. Chem. A* **2016**, *4*, 3371.
14. L. Guo, J. Feng, Z. Fang, J. Xu, X. Lu, *Trends Food Sci. Technol.* **2015**, *46*, 252.
15. J. Y. Yoon, B. Kim, *Sensors* **2012**, *12*, 10713.
16. M. Guix, C. C. Mayorga-Martinez, A. Merkoçi, *Chem. Rev.* **2014**, *114*, 6285.
17. C. Luni, H. C. Feldman, M. Pozzobon, P. De Coppi, C. D. Meinhart, N. Elvassore, *Biomicrofluidics* **2010**, *4*, 034105.
18. T. Takei, S. Sakoguchi, M. Yoshida, *J. Biosci. Bioeng.* **2018**, *126*, 649.
19. K. K. Dey, F. Wong, A. Altemose, A. Sen, *Curr. Opin. Colloid Interface Sci.* **2016**, *21*, 4.
20. J. Li, I. Rozen, J. Wang, *ACS Nano* **2016**, *10*, 5619.
21. M. Uygun, V. V. Singh, K. Kaufmann, D. A. Uygun, S. D. de Oliveira, J. Wang, *Angew. Chem.* **2015**, *127*, 13092.
22. R. F. Ismagilov, A. Schwartz, N. Bowden, G. M. Whitesides, *Angew. Chem.* **2002**, *4*, 652-654.
23. J. Wang, *Lab on a chip* **2012**, *12*, 1944.
24. S. Ebbens, *Cur. Opin. Colloid & Interface Sci.* **2016**, *21*, 14.
25. J. Orozco, B. Jurado-Sánchez, G. Wagner, W. Gao, R. Vazquez-Duhalt, S. Sattayasamitsathit, M. Galarnyk, A. Cortés, D. Saintillan, J. Wang, *Langmuir* **2014**, *30*, 5082.
26. E. Morales-Narváez, M. Guix, M. Medina-Sánchez, C. C. Mayorga-Martinez, A. Merkoçi, *Small* **2014**, *10*, 2542.
27. S. Das, A. Garg, A. I. Campbell, J. Howse, A. Sen, D. Velegol, R. Golestanian, S. J. Ebbens, *Nat. commun.* **2015**, *6*, 8999.
28. K. K. Dey, X. Zhao, B. M. Tansi, W. J. Méndez-Ortiz, U. M. Córdova-Figueroa, R. Golestanian, A. Sen, *Nano lett.* **2015**, *15*, 8311.
29. X. Lin, Z. Wu, Y. Wu, M. Xuan, Q. He, *Adv. Mater.* **2016**, *28*, 1060.
30. R. Archer, A. Campbell, S. J. Ebbens, *Soft Matter* **2015**, *11*, 6872.
31. C. A. Sternling, L. Scriven, *AIChE J.* **1959**, *5*, 514.
32. H. Hu, R. G. Larson, *J. Phys. Chem. B* **2006**, *110*, 7090.
33. N. J. Suematsu, T. Sasaki, S. Nakata, H. Kitahata, *Langmuir* **2014**, *30*, 8101.
34. D. Patra, S. Sengupta, W. Duan, H. Zhang, R. Pavlick, A. Sen, *Nanoscale* **2013**, *5*, 1273.
35. D. A. Gregory, Y. Zhang, P. J. Smith, X. Zhao, S. J. Ebbens, *Small* **2016**, *12*, 4048.
36. T. Y. Huang, M. S. Sakar, A. Mao, A. J. Petruska, F. Qiu, X. B. Chen, S. Kennedy, D. Mooney, B. J. Nelson, *Adv. Mater.* **2015**, *27*, 6644.
37. W. Zhu, J. Li, Y. J. Leong, I. Rozen, X. Qu, R. Dong, Z. Wu, W. Gao, P. H. Chung, J. Wang, *Adv. mater.* **2015**, *27*, 4411.
38. L. K. Abdelmohsen, M. Nijemeisland, G. M. Pawar, G.J. A. Janssen, R. J. Nolte, J. C. van Hest, D. A. Wilson, *ACS Nano* **2016**, *10*, 2652.
39. T. Ranzani, S. Russo, N. W. Bartlett, M. Wehner, R. J. Wood, *Adv. Mater.* **2018**, *30*, 1.
40. W. Gao, S. Sattayasamitsathit, J. Orozco, J. Wang, *Nanoscale* **2013**, *5*, 8909.
41. M. Sridhar, C. R. Reddy, *Environ. Pollut., Ser. B* **1984**, *7*, 49.

Figures:

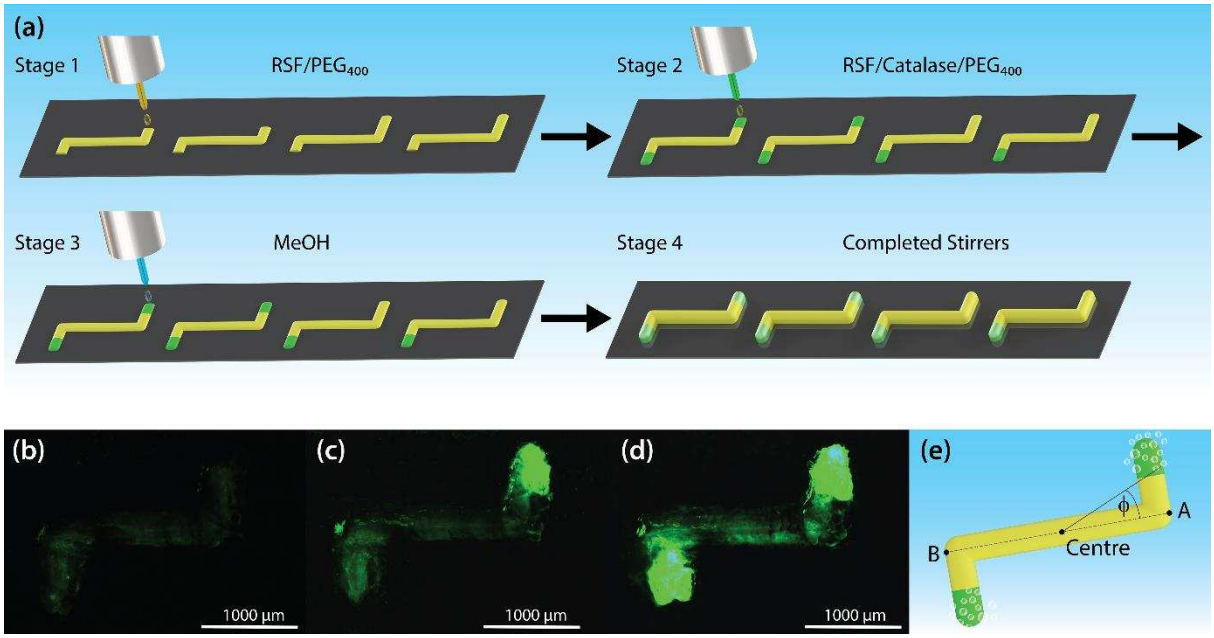

Figure 1. **(a)** A schematic representing the procedure of layer-by-layer reactive inkjet printing of regenerated silk fibroin (RSF) stirrers. Ink A: RSF/PEG_{400} mixture (yellow), ink B: RSF/Catalase/PEG_{400} mixture (green) and ink C: methanol curing ink (blue). *Stage 1*: Printing of ink A in order to build the main body of the silk stirrers. *Stage 2*: Printing of ink B for the 'engine' part of the silk stirrers containing catalase. *Stage 3*: Printing ink C (methanol) to transform printed RSF from soluble random coil structure into insoluble beta-sheet structure. *Stage 4*: Stages 1 to 3 are repeated consecutively to form 3D structures. The height of the structures is determined by the number of layers printed. **(b-d)** Fluorescent microscopy images of silk stirrers (Catalase was labelled with FITC which appears green. The fluorescence from the main bodies is mainly due to the auto-fluorescence of the silk material rather than catalase). Stirrer dimensions: 2000 µm in length 900 µm arms and 90 µm in height. **(b)** No catalase presents. **(c)** Catalase printed on one end only (single-engine). **(d)** Catalase printed on both ends (dual-engine). **(e)** A schematic of silk stirrer indicating tracking points A and B and angle of orientation (ϕ), green regions indicate catalase doped silk regions.

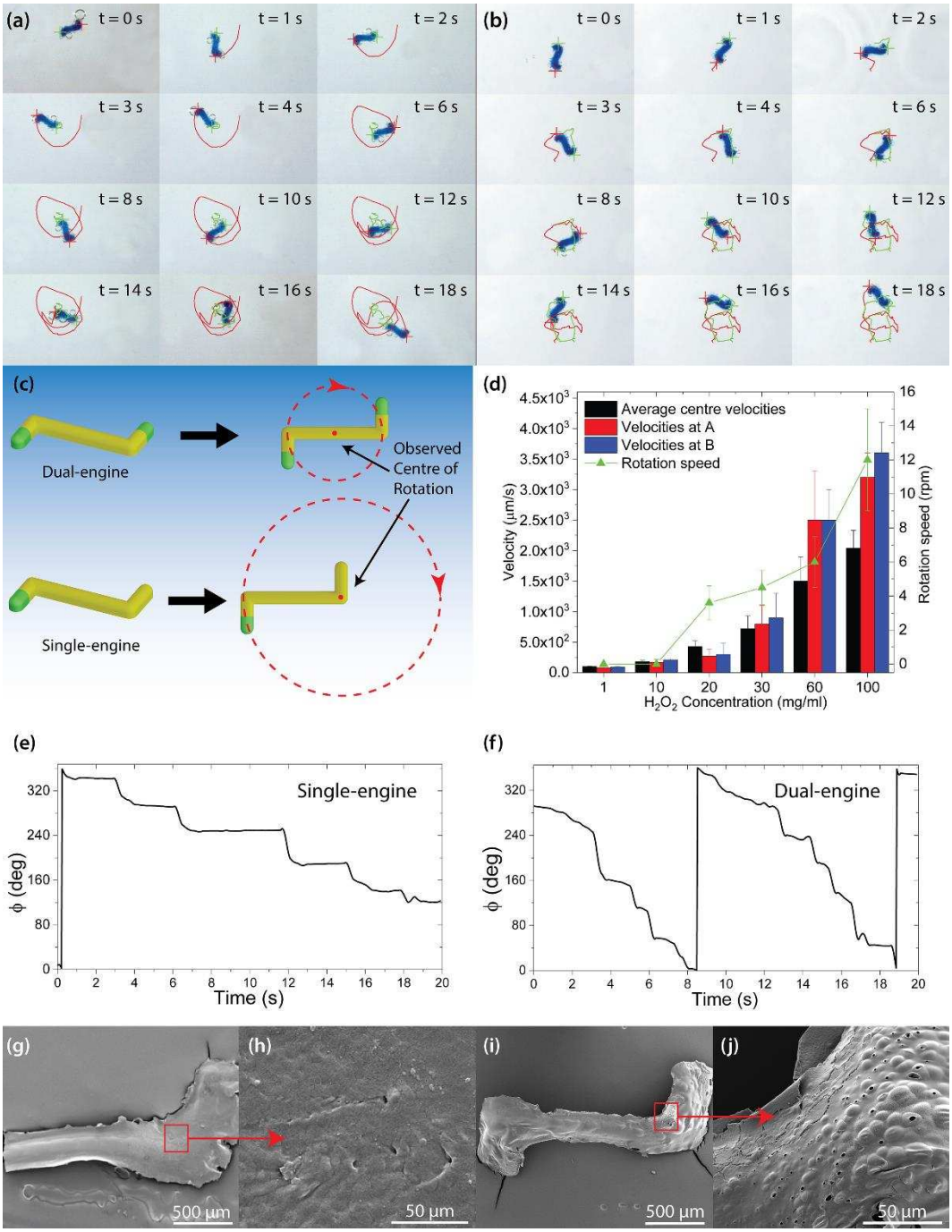

Figure 2. **(a and b)** Still video frames from catalase stirrers in 60 mg/ml H_2O_2 solutions for **(a)** a single-engine stirrer and **(b)** a dual-engine stirrer (**video S1** and **S2**, supporting information). **(c)** Schematic representations of dual-engine and single-engine silk stirrers, illustrating the observed centre of rotation during stirring action. **(d)** The effect of H_2O_2 fuel concentration on the velocity (measured at the points A and B shown in Figure 1e) and rotation speed of dual-engine silk stirrers. **(e and f)** Representative graphs showing the angle of orientation ϕ over time for a single-engine stirrer **(e)** and a dual-engine stirrer **(f)** in 60 mg/ml of H_2O_2 fuel solutions. **(g-j)** SEM images of silk stirrers: **(g and h)** before H_2O_2 exposure. **(i and j)** after H_2O_2 exposure. **(j)** Enlargement showing porous structure on the catalase containing region of the same stirrer.

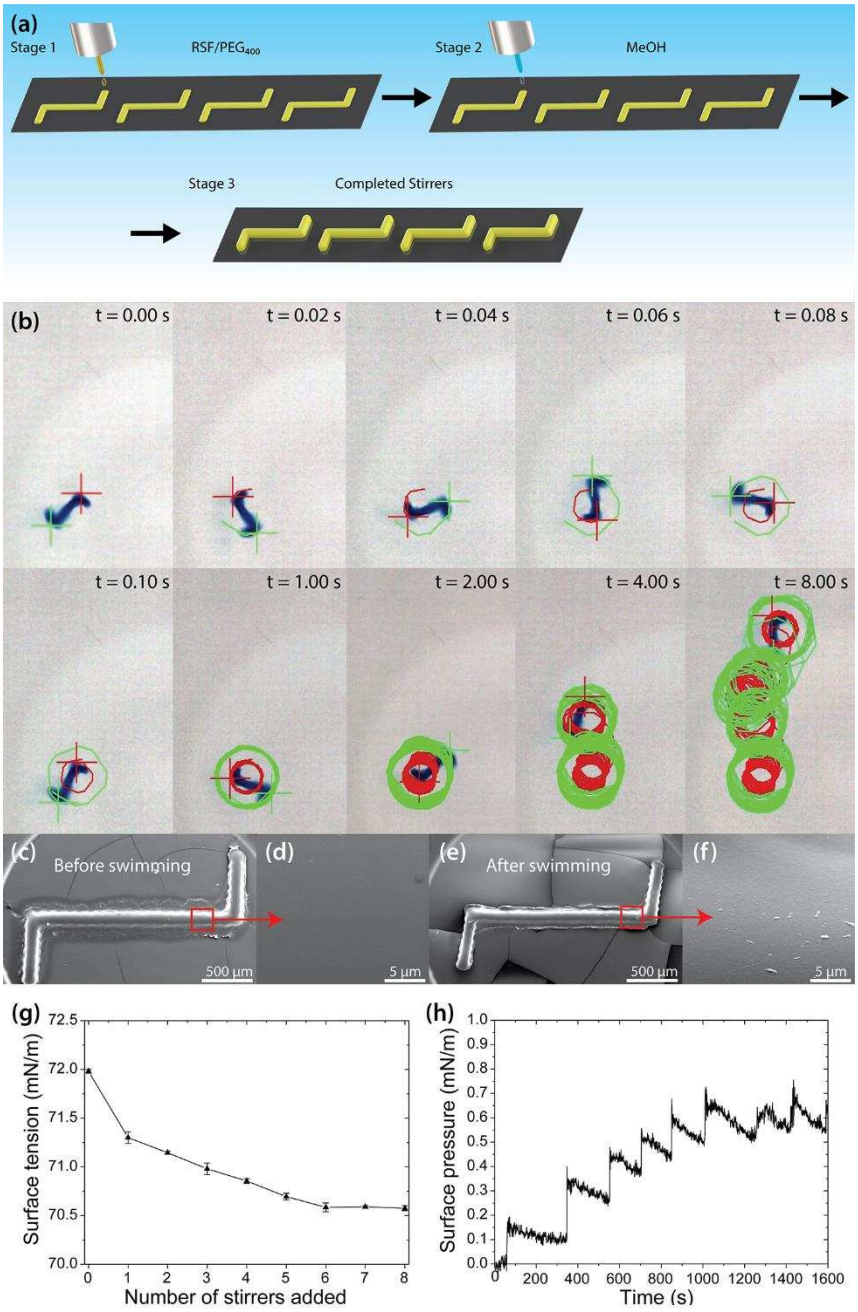

Figure 3. **(a)** A schematic representing the layer-by-layer reactive inkjet printing procedure of regenerated silk fibroin (RSF) / PEG_{400} stirrers. Ink D: RSF/PEG_{400} mixture (yellow) and ink C: methanol curing ink (blue). Stage 1: Printing of ink D in order to build the body of the silk stirrers. Stage 2: Printing of ink C (methanol ink) to transform printed silk ink from soluble random coil structure into insoluble β-sheet structure. Stage 3: Stages 1 to 2 are repeated consecutively to form 3D structures. The height of the structures is determined by the number of layers printed. **(b)** Still video frames of a Marangoni effect powered stirrer (100 layers) in DI water undergoing surface tension motion (**Video S4**, supporting information). Red and Green lines show the trajectories at the two ends of the stirrer. **(c-f)** SEM images of stirrers before **(c & d)** and after **(e & f)** interaction with DI water. **(g)** Change of surface tension as a function of number of stirrers added. **(h)** Change of surface pressure as a function of time, each peak corresponds to an additional stirrer being added to the interface on the Langmuir trough.

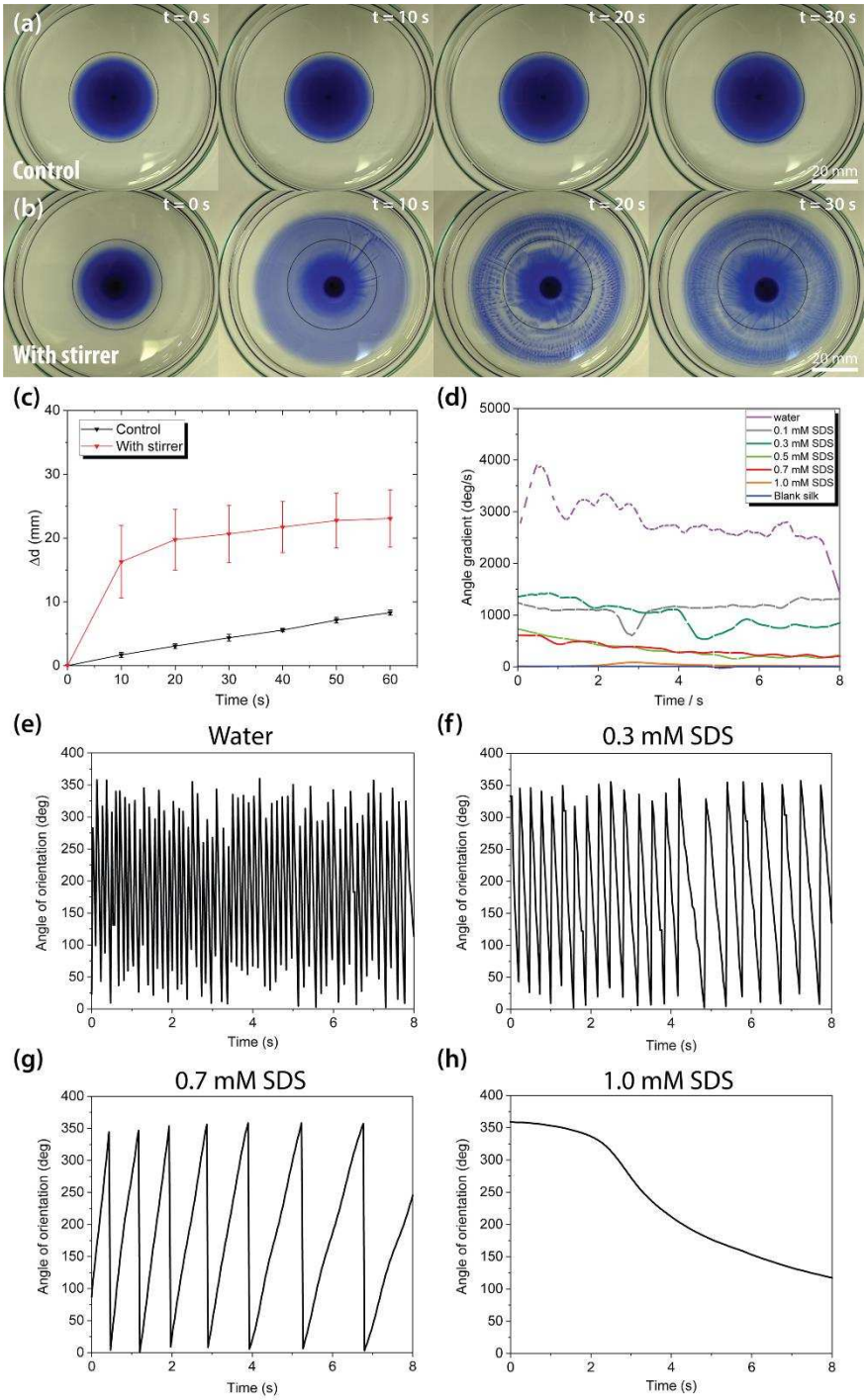

Figure 4. **(a & b)** Demonstration of the stirring effect using Marangoni effect powered silk stirrers, data for at least 3 stirrers was collected to verify representative results (**Video S5**, supporting information). **(a)** is a control (without stirrer) **(b)** with silk/PEG stirrer. The blue dye is a mixture of glycerol and blue fountain pen ink at a ratio of 1:1, in a glass petri dish of 9 cm diameter. **(c)** The change of diameter of the dye circle as a function of time, comparing the dye diffusion with and without a silk stirrer. **(d)** The comparison of angle gradients of stirrers added in a series of SDS solutions with different concentrations. **(e-h)** The comparison of angle of orientation (rotation) of stirrers added in a series of SDS solutions with different concentrations, where: **(e)** Water (surface tension: 72.0 mN/m), **(f)** 0.3 mM SDS (surface tension: 70.5 mN/m), **(g)** 0.7 mM SDS (surface tension: 68.8 mN/m), **(h)** 1.0 mM SDS (surface tension: 66.9 mN/m). Please see **Video S6-S10**, supporting information for further illustration of the surface tension effect.

The table of contents entry:

This paper reports the ability of inkjet printed silk micro-stirrers to enhance mixing in small volumes of fluid. The micro-stirrers can produce rotation by releasing a surface active additive, or by the surface detachment of enzymatically generated bubbles. The devices can also be used as motion sensors for detecting surface tension modifying water pollutants.

Keyword

Yu Zhang, David A. Gregory, Yi Zhang, Patrick J. Smith, Stephen J. Ebbens, and Xiubo Zhao*

Title: Reactive Inkjet Printing of Functional Silk Stirrers for Enhanced Mixing and Sensing

ToC figure

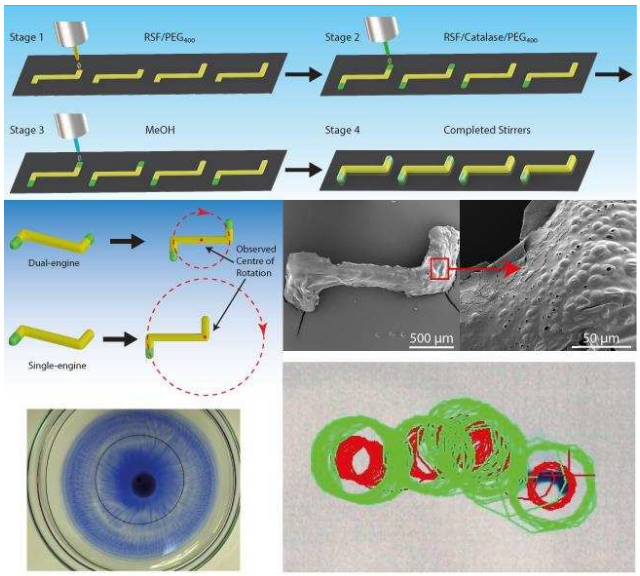

Copyright WILEY-VCH Verlag GmbH & Co. KGaA, 69469 Weinheim, Germany, 2016.